Scotogenic top-quark FCNC decays

Chuan-Hung Chen[1,2,*] and Takaaki Nomura[3,†]

[1]*Department of Physics, National Cheng-Kung University, Tainan 70101, Taiwan*
[2]*Physics Division, National Center for Theoretical Sciences, Taipei 10617, Taiwan*
[3]*College of Physics, Sichuan University, Chengdu 610065, China*

(Received 16 April 2022; revised 7 October 2022; accepted 14 October 2022; published 3 November 2022)

Flavor-changing neutral current (FCNC) top-quark decays are highly suppressed due to the Glashow-Iliopoulos-Maiani mechanism in the standard model (SM). If $t \to qh, qV$ with $V = g, \gamma, Z$ are all induced via quantum loop levels, then we investigate the effect that can enhance the top-FCNC up to the sensitivity designed at the high-luminosity (HL) LHC. Inspired by the mechanism of the scotogenic neutrino mass, we extend the SM by including Z_2-odd colored fermions when a Z_2 discrete is imposed. The results show that by taking $\mathrm{BR}(t \to ug) \lesssim 0.61 \times 10^{-4}$ recently measured by ATLAS as an input, $t \to q\gamma$ can be indirectly bounded to be $\mathrm{BR}(t \to q\gamma) \lesssim 3.2 \times 10^{-6}$, which is below the expected sensitivity at the HL LHC. After taking potential constraints from various experiments into account, the obtained branching ratios for the loop-induced $t \to qh$ and $t \to qZ$ decays can be $O(10^{-4})$, which falls within the sensitivity at the HL LHC.

DOI: 10.1103/PhysRevD.106.095005

I. INTRODUCTION

Flavor-changing neutral currents (FCNCs) are suppressed at the tree level and can be induced via quantum corrections in the standard model (SM). However, loop-induced top-quark FCNCs are highly suppressed in the SM due to the Glashow-Iliopoulos-Maiani (GIM) mechanism [1]. As a result, the branching ratios (BRs) for the $t \to q(g, \gamma, Z, h)$ decays with $q = u, c$ in the SM are of the order of $10^{-12} - 10^{-17}$ [2–4], and the results are far below the LHC sensitivities.

The expected sensitivities in the high-luminosity (HL) LHC with an integrated luminosity of 3 ab^{-1} at $\sqrt{s} =$ 14 TeV are expected to be 2.4–5.8 $\times 10^{-5}$ for $t \to qZ$ [5], 1.5×10^{-4} for $t \to qh$ [6], and $0.9 - 7 \times 10^{-5}$ for $t \to q\gamma$ [7]. The event that the top-FCNC is found at the 10^{-5} level definitely indicates a new physics effect. Thus, the top-quark flavor-changing processes can serve as good candidates for investigating new physics effects. To explore the new physics effects in the rare top-quark decays, various extensions of the SM, which can reach the HL LHC sensitivity, were proposed in [8–26].

The top-FCNC effects not only can be detected via the new top-quark decay channels, but also can be used to produce more top-quark events, such as $gq \to t$. Using the single-top production, the upper limits on the BR using 139 fb^{-1} at $\sqrt{s} = 13$ TeV in ATLAS are shown as $\mathrm{BR}(t \to ug) < 0.61 \times 10^{-4}$ and $\mathrm{BR}(t \to cg) < 3.7 \times 10^{-4}$ [27].

If all mentioned top-FCNC processes are enhanced via quantum loop effects, the intermediate states in the loops may carry the quantum number that the SM particles do not possess. A known example is the radiative neutrino mass in a scotogenic model [28], where the mediated particles in the loop are Z_2-parity odd, whereas the SM particles are Z_2-parity even. Interestingly, in addition to the explanation of the neutrino mass, the predicting dark matter (DM) candidate can fit the DM relic density that was observed by the Planck Collaboration [29].

If we have Z_2-odd colorless fermions, it is reasonable that there also exist Z_2-odd colored fermions, which are similar to the quarks in the SM. Hereafter, we call these particles as Z_2-odd quarks. Based on this assumption, when we make a minimal extension of the Ma-model proposed in [28], we investigate if the top-FCNC processes can be enhanced up to the sensitivities of the HL LHC. As the minimal requirement, no new local gauge symmetry is considered, and the number of including Z_2-odd quarks is as less as possible. Since a new local gauge symmetry introduces a new gauge coupling and gauge boson(s), which are not directly related to the top-FCNC processes, thus, we only focus on the SM gauge symmetry.

Because the $t \to q\gamma(h)$ decay involves the structure of a dipole (scalar) current, the chirality in the initial and final quarks has to be different. In addition, the left-handed and right-handed top quarks are $SU(2)$ doublet and singlet in the SM, respectively. Therefore, to avoid the chirality

*physchen@mail.ncku.edu.tw
†nomura@scu.edu.cn

suppression of m_t^2/Λ^2, where Λ is the mass scale of the new heavy particle, the candidate of new colored fermions should be chosen in such a way that the chirality suppression can be overcome. Without introducing extra new Z_2-odd scalar field with the exception of the inert Higgs doublet, we find that the possibly minimal representations for the colored fermions in $SU(2)_L \times U(1)_Y$ gauge symmetry are the vectorlike doublet and singlet. Vectorlike particles are used because their gauge anomaly can be evaded.

Three scalar bosons exist in an inert Higgs doublet, namely, inert charged Higgs, scalar, and pesudoscalar, where the lightest neutral inert scalar can be the DM candidate. Due to the suppression factor of m_t^2/Λ^2, which arises from the chirality flip of top-quark, the contributions from the neutral inert scalars to $t \to qh$ are small; therefore, the $t \to qh$ processes are dominated by the inert charged Higgs. Although $t \to q\gamma$ can avoid the chirality suppression, since the loop-induced effect is associated with the mixing between Z_2-odd doublet and singlet quark, which is of order of v/Λ with v being the vacuum expectation value of Higgs field, $t \to q\gamma$ dominated by the inert charged Higgs in the model cannot be enhanced up to the sensitivity of HL LHC. For the $t \to qZ$ processes, both neutral and charged scalars can have significant contributions.

The remainder of this paper is organized as follows: We introduce the model and derive the relevant Yukawa and gauge couplings in Sec. II. Based on the obtained couplings, we formulate the decay amplitudes and BRs for the studied top decays in Sec. III. Then, we discuss various possible constraints, which include radiative B-meson decay, oblique parameters, Higgs production, and DM detections, in Sec. IV. We analyze and discuss the numerical results in detail in Sec. V. Finally, we summarize the study in Sec. VI.

II. MODEL AND THE NEW COUPLINGS

To enhance the top-quark FCNC processes through radiative corrections without introducing a new gauge symmetry in a scotogenic mechanism, we impose a Z_2 discrete symmetry in the model and extend the SM, including a new Higgs doublet (Φ_I), three singlet Majorana fermions N_{Ri} $(i = 1\text{–}3)$ and vectorlike quark doublet (Q_4) and singlet (B'), where the introduced particles are Z_2-odd and the SM particles are Z_2-even under the Z_2 transformation. The representations and charge assignments of new particles in $SU(2)_L \times U(1)_Y \times Z_2$ are shown in Table I. The Z_2 odd Majorana fermions N_Rs are necessary to generate neutrino mass by scotogenic mechanism. In this work we do not discuss neutrino mass generation since it is exactly the same as original Ma-model [28]. Due to the unbroken Z_2 symmetry, the neutral component of the inert Higgs doublet and the lightest Majorana fermion can be the DM candidate [30]. Since the inert Higgs doublet is directly related to the top-FCNC process, in this study, we take the lightest neutral component of Φ_I as the DM candidate. We derive the relevant couplings for top-quark FCNC in the following discussions.

TABLE I. Representations and charge assignments for new particles.

	$SU(3)_C$	$SU(2)_L$	$U(1)_Y$	Z_2
Q_4	3	2	1/3	−1
B'	3	1	−2/3	−1
Φ_I	1	2	1/2	−1
N_{Ri}	1	1	0	−1

A. Yukawa couplings and scalar potential

Based on the charge assignments shown in Table I, the new Yukawa interactions can be written as

$$\begin{aligned}-\mathcal{L}_Y = {} & y_{B'}\overline{Q_{4L}}HB'_R + \tilde{y}_{B'}\overline{Q_{4R}}HB'_L + \overline{Q_{4L}}\mathbf{Y}_I^d\Phi_I d_R \\ & + \overline{Q_{4L}}\mathbf{Y}_I^u\widetilde{\Phi}_I u_R + \overline{Q_L}\mathbf{Y}_I^{B'}\Phi_I B'_R + m_{4Q}\overline{Q_{4L}}Q_{4R} \\ & + m_{B'}\overline{B'_L}B'_R + \text{H.c.}, \end{aligned} \tag{1}$$

where the flavor indices are suppressed; $\tilde{\Phi}_I = i\tau_2\Phi_I^*$ and τ_2 is the Pauli matrix, and H is the SM Higgs doublet. In this work, we considered that the new Yukawa couplings are real. Since Eq. (1) does not involve the SM quark mass diagonalization, the up- and down-type quarks can be taken as the physical states, and the flavor mixing effects are absorbed into the Yukawa couplings. The doublet components of Q_4, Φ_I, and H are taken as

$$\begin{aligned} Q_4 = \begin{pmatrix} T \\ B \end{pmatrix}, \qquad \Phi_I = \begin{pmatrix} H_I^+ \\ \frac{1}{\sqrt{2}}(H_I + iA_I) \end{pmatrix}, \\ H = \begin{pmatrix} G^+ \\ \frac{1}{\sqrt{2}}(v + h + iG^0) \end{pmatrix}. \end{aligned} \tag{2}$$

Thus, the first two terms in Eq. (1) lead to the mixture between B and B', and the associated mass matrix is expressed as

$$(\overline{B}', \bar{B})_L \begin{pmatrix} m_{B'} & \frac{\tilde{y}_{B'}v}{\sqrt{2}} \\ \frac{y_{B'}v}{\sqrt{2}} & m_{4Q} \end{pmatrix} \begin{pmatrix} B' \\ B \end{pmatrix}_R. \tag{3}$$

In general, we need biunitary transformation to diagonalize the mass matrix in Eq. (3). In order to simplify the analysis, we take $\tilde{y}_{B'} = y_{B'}$ and the 2×2 real symmetric matrix can be diagonalized by an $SO(2)$ transformation, where the eigenvalues and eigenstates can be obtained as

$$m_{B_{1(2)}} = \frac{m_{4Q}+m_{B'}}{2} \mp \frac{1}{2}\sqrt{(m_{4Q}-m_{B'})^2+2y_{B'}^2v^2},$$
$$\begin{pmatrix} B_1 \\ B_2 \end{pmatrix} = \begin{pmatrix} \cos\theta & -\sin\theta \\ \sin\theta & \cos\theta \end{pmatrix}\begin{pmatrix} B' \\ B \end{pmatrix},$$
$$\tan 2\theta = \frac{\sqrt{2}y_{B'}v}{m_{4Q}-m_{B'}}, \tag{4}$$

where θ is the mixing angle of B and B'. We have taken B_1 as the lightest Z_2-odd quark. The resulting Yukawa couplings are then written as

$$\mathcal{L}_Y \supset \bar{B}_1(-s_\theta \mathbf{Y}_I^u P_R - c_\theta \mathbf{Y}_I^{B'} P_L)uH_I^- + \bar{B}_2(c_\theta \mathbf{Y}_I^u P_R - s_\theta \mathbf{Y}_I^{B'} P_L)uH_I^- - \frac{1}{\sqrt{2}}\bar{T}\mathbf{Y}_I^u P_R u(H_I - iA_I)$$
$$-\frac{1}{\sqrt{2}}(c_\theta \bar{B}_1 + s_\theta \bar{B}_2)\mathbf{Y}_I^{B'} P_L d(H_I - iA_I) - \bar{T}\frac{\mathbf{Y}_I^d}{\sqrt{2}}P_R dH_I^+ - (-s_\theta \bar{B}_1 + c_\theta \bar{B}_2)\frac{\mathbf{Y}_I^d}{\sqrt{2}}P_R d(H_I + iA_I) + \text{H.c.}, \tag{5}$$

with $c_\theta(s_\theta) = \cos\theta(\sin\theta)$. Using the parametrization, the Higgs couplings to B_1 and B_2 can be written as

$$\mathcal{L}_{hBB} = -\frac{1}{\sqrt{2}}h(\bar{B}_1, \bar{B}_2)\mathbf{y}^h\begin{pmatrix} B_1 \\ B_2 \end{pmatrix}$$
$$= -\frac{y_{B'}}{\sqrt{2}}h(\bar{B}_1, \bar{B}_2)\begin{pmatrix} -s_{2\theta} & c_{2\theta} \\ c_{2\theta} & s_{2\theta} \end{pmatrix}\begin{pmatrix} B_1 \\ B_2 \end{pmatrix}, \tag{6}$$

with $c_{2\theta}(s_{2\theta}) = \cos 2\theta(\sin 2\theta)$. The hB_iB_i coupling, which will lead to the $t \to qh$ decay at the loop level, can be induced from the mixing terms of B_1 and B_2. We note that there is no hTT coupling at the tree level in the model.

The masses of the inert scalars and their couplings to the Higgs are determined by the scalar potential, which can be written as [28,30]

$$V(H,\Phi_I) = \mu_1^2 H^\dagger H + \mu_2^2 \Phi_I^\dagger \Phi_I + \lambda_1 (H^\dagger H)^2 + \lambda_2 (\Phi_I^\dagger \Phi_I)^2$$
$$+ \lambda_3 (H^+ H)(\Phi_I^\dagger \Phi_I) + \lambda_4 (H^+ \Phi_I)(\Phi_I^\dagger H)$$
$$+ \left[\frac{1}{2}\lambda_5 (H^\dagger \Phi_I)^2 + \text{H.c.}\right]. \tag{7}$$

We can obtain the mass squares of $H_I^\pm$, H_I, and A_I as

$$m_{H_I}^2 = \mu_2^2 + \frac{\lambda_L v^2}{2}, \quad m_{A_I}^2 = \mu_2^2 + \frac{\lambda_A v^2}{2}, \quad m_{H_I^\pm}^2 = \mu_2^2 + \frac{\lambda_3 v^2}{2}, \tag{8}$$

with $\lambda_{L(A)} = \lambda_3 + \lambda_4 \pm \lambda_5$. The mass difference between H_I and A_I depends on the λ_5 parameter. The Higgs couplings to $(H_I^\pm, H_I, A_I)$ can be determined as

$$hH_I^+H_I^- : \lambda_3 v, \qquad hH_IH_I : \lambda_L v, \qquad hA_IA_I : \lambda_A v. \tag{9}$$

In addition to the minimal conditions, i.e., $\partial V/\partial h(H_I) = 0$, the vacuum stability is controlled by the copositivity criteria in the dimension-4 terms of scalar potential, and the stable conditions are yielded as [30–32]

$$\lambda_{1,2} \geq 0, \qquad \lambda_3 + 2\sqrt{\lambda_1\lambda_2} \geq 0,$$
$$\lambda_3 + \lambda_4 - |\lambda_5| + 2\sqrt{\lambda_1\lambda_2} \geq 0. \tag{10}$$

If we take the mass ordering to be $m_{H_I^\pm} > m_{A_I} > m_{H_I}$, then $\lambda_{4,5} < 0$, which can be expressed as

$$|\lambda_4| = \frac{1}{v^2}(2m_{H_I^\pm}^2 - m_{H_I}^2 - m_{A_I}^2), \quad |\lambda_5| = \frac{m_{A_I}^2 - m_{H_I}^2}{v^2}. \tag{11}$$

To obtain the potential bounded from below, where the conditions in Eq. (10) are satisfied, we require $\lambda_3 > 0$. Thus, some cancellation occurs in the hS_IS_I ($S_I = H_I, A_I$) coupling. In addition, in Eq. (5), S_ITu couplings are only associated with the right-handed up-type SM quarks. As a result, the loop-induced $t \to q(h,\gamma)$ processes through the S_ITu couplings are suppressed by m_i^2/m_T^2, and they are negligible if $m_T \sim O(1)$ TeV. Hence, when the heavy quark and inert Higgs masses are fixed, the main parameters that affect the rare top decays in the model are the Yukawa couplings $\mathbf{Y}_I^{B'}$ and $\mathbf{Y}_I^u$, the mixing angle θ, and the λ_3 parameter that is directly related to the $hH_I^-H_I^+$ coupling.

B. Gauge couplings to new fermions and scalars

To study the $t \to qV$ ($V = \gamma, Z$) processes, we also need the gauge couplings of the photon and Z-boson to the inert Higgses and to the Z_2-odd quarks, where the gauge couplings from the kinetic terms of H_I, Q_4, and B' are written as

$$\mathcal{L}_{\text{gauge}} \supset (D_\mu \Phi_I)^\dagger D^\mu \Phi_I + \overline{Q_4} i\not{D} Q_4 + \overline{B'} i\not{D} B'. \tag{12}$$

The covariant derivatives for the doublet and singlet fields are taken as

$$D^\mu = \partial^\mu + ig\vec{T}\cdot\vec{W}^\mu + ig'\frac{Y}{2}B_\mu,$$
$$D'^\mu = \partial^\mu + ig'\frac{Y}{2}B_\mu, \tag{13}$$

where $W^{i\mu}$ and B^μ are the gauge fields of $SU(2)_L$ and $U(1)_Y$, respectively. Using the standard notations for the photon and Z-boson, which are defined as

$$A_\mu = c_W B_\mu + s_W W^3_\mu,$$
$$Z_\mu = -s_W B_\mu + c_W W^3_\mu. \tag{14}$$

The neutral gauge couplings to the inert Higgses are obtained as

$$\mathcal{L}_{VS_IS_I} \supset i\left(eA^\mu + \frac{gc_{2W}}{2c_W}Z^\mu\right)(H_I^+\partial_\mu H_I^- - H_I^-\partial_\mu H_I^+) + \frac{g}{2c_W}Z^\mu(A_I\partial H_I - H_I\partial_\mu A_I), \tag{15}$$

where $c_W(s_W) = \cos\theta_W(\sin\theta_W)$, and θ_W is the Weinberg's angle. Since the quark T doesn't mix with the SM up-type quarks, its gauge couplings to the photon and the Z boson can be simply written as

$$-eQ_t\bar{T}\gamma_\mu T A^\mu - \frac{g}{c_W}\left(\frac{1}{2} - Q_t s_W^2\right)\bar{T}\gamma_\mu T Z^\mu. \tag{16}$$

Although the photon couplings to B_1 and B_2 are flavor conserved, since the B and B' quarks belong to different $SU(2)_L$ representations and are mixed via the Yukawa couplings, their Z gauge couplings allow flavor-changing and are expressed as

$$\mathcal{L}_{VBB} = -eQ_b\sum_i \bar{B}_i\gamma_\mu B_i A^\mu - \frac{g}{c_W}(\bar{B}_1,\bar{B}_2)\gamma_\mu \mathbf{C}^Z\begin{pmatrix}B_1\\B_2\end{pmatrix}Z^\mu, \tag{17}$$

with

$$\mathbf{C}^Z = \begin{pmatrix}-s_\theta^2/2 - Q_b s_W^2 & s_\theta c_\theta\\ s_\theta c_\theta & -c_\theta^2/2 - Q_b s_W^2\end{pmatrix}. \tag{18}$$

Because the charged gauge boson $W^\pm$ only couples to the doublet quarks, the $W^\pm$ coupling can be found as

$$\mathcal{L}_{WTB} = -\frac{g}{\sqrt{2}}\bar{T}\gamma_\mu(-s_\theta B_1 + c_\theta B_2)W^{+\mu} + \text{H.c.} \tag{19}$$

III. LOOP-INDUCED DECAY AMPLITUDES FOR $t \to q(h,V)$

In this section we derive the decay amplitudes for the $t \to q(h,V)$ decays. Because the calculations for $t \to qg$ are similar to those for $t \to q\gamma$, and their BRs can be approximately related by $\text{BR}(t \to qg) \sim C_F(\alpha_s/\alpha)\text{BR}(t \to q\gamma)$ with $C_F = 4/3$ in the model, where $\alpha = e^2/4\pi$ and $\alpha_s = g_s^2/4\pi$. In this study, we only focus on the $t \to q\gamma$ analysis.

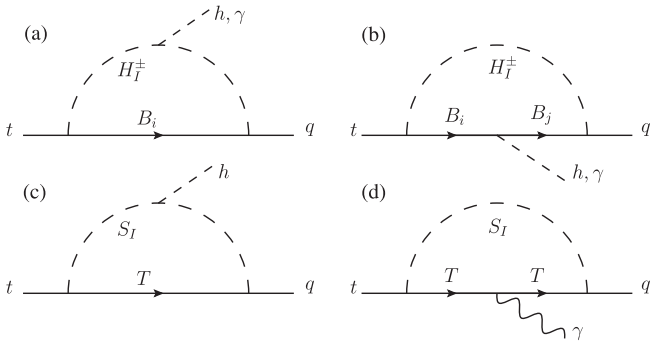

FIG. 1. Feynman diagrams used to induce the $t \to q(h,\gamma)$ processes, where the emitted dashed lines can be the Higgs or photon.

A. $t \to q(h,\gamma)$ decays

In the model, the $t \to q(h,\gamma)$ processes can be induced from the loops with the mediation of $H_I^\pm$ and S_I. The Feynman diagrams are sketched in Fig. 1, where the emitted dashed lines can be the Higgs or the photon. Since there is no hTT coupling, the $t \to qh$ decay cannot be produced from Fig. 1(d). In Fig. 1(b), the flavor-changing between B_1 and B_2 only occurs in the Higgs coupling.

The effective interactions for $t \to q(h,\gamma)$ can be written as

$$\mathcal{L}_{t\to q(h,\gamma)} = -C_L^h\bar{q}P_L t h - C_R^h\bar{q}P_R t h + \frac{eB_L^\gamma}{m_t}\bar{q}i\sigma_{\mu\nu}\epsilon_\gamma^{\mu*}k^\nu P_L t + \frac{eB_R^\gamma}{m_t}\bar{q}i\sigma_{\mu\nu}\epsilon_\gamma^{\mu*}k^\nu P_R t. \tag{20}$$

Following the Feynman diagrams shown in Fig. 1 and the couplings obtained in Eqs. (5) and (15)–(17), the effective Wilson coefficients with $\chi = L, R$ can be written as

$$C_\chi^h = \sum_i\left(C_{i\chi}^{ha} + \sum_j C_{ij\chi}^{hb}\right) + C_\chi^{hc},$$
$$B_\chi^\gamma = \sum_i(B_{i\chi}^{\gamma a} + B_{i\chi}^{\gamma b}) + B_\chi^{\gamma d}. \tag{21}$$

The contributions to $t \to qh$ from each diagram can be formulated as

$$
\begin{aligned}
C_{iL}^{ha} &= \frac{\lambda_3 v}{(4\pi)^2 m_t} C_{iR}^{q} \int_0^1 dx_1 \int_0^{x_1} dx_2 \frac{C_{iR}^{t} r_{it} x_2 + \sqrt{r_{it}} C_{iL}^{t}}{D_h^a(r_{iH_I^\pm}, r_{it}, r_{ih})}, \\
C_{iR}^{ha} &= \frac{\lambda_3 v}{(4\pi)^2 m_t} C_{iL}^{q} \int_0^1 dx_1 \int_0^{x_1} dx_2 \frac{C_{iL}^{t} r_{it} x_2 + C_{iR}^{t} \sqrt{r_{it}}}{D_h^a(r_{iH_I^\pm}, r_{it}, r_{ih})}, \\
C_{ijL}^{hb} &= -\frac{y_{ij}^{h}}{(4\pi)^2} \int_0^1 dx_1 \int_0^{x_1} dx_2 \frac{C_{jR}^{q}}{D_h^b(r_{jH_I^\pm}, r_{jt}, r_{ji}, r_{jh})} [C_{iR}^{t}(r_{jt} x_2 (1-x_1) \\
&\quad + r_{jh}(x_1 - x_2) - r_{ji}) + C_{iL}^{t} \sqrt{r_{jt}} (\sqrt{r_{jt}} x_2 - (1-x_2))], \\
C_{ijR}^{hb} &= -\frac{y_{ij}^{h}}{(4\pi)^2} \int_0^1 dx_1 \int_0^{x_1} dx_2 \frac{C_{jL}^{q}}{D_h^b(r_{jH_I^\pm}, r_{jt}, r_{ji}, r_{jh})} [C_{iL}^{t}(r_{jt} x_2 (1-x_1) \\
&\quad + r_{jh}(x_1 - x_2) - r_{ji}) + C_{iR}^{t} \sqrt{r_{jt}} (\sqrt{r_{jt}} x_2 - (1-x_2))], \\
C_{L}^{hc} &= \frac{Y_{Iq}^{u} Y_{I3}^{u} y_t}{(4\pi)^2} \frac{v}{m_t} \int_0^1 dx_1 \int_0^{x_1} dx_2 x_2 \left[\frac{\lambda_3 + \lambda_4 + 2\lambda_5}{D_h^a(y_{H_I}, y_t, y_h)} + \frac{\lambda_3 + \lambda_4 + -2\lambda_5}{D_h^a(y_{A_I}, y_t, y_h)} \right],
\end{aligned}
\tag{22}
$$

where $r_{if} = m_f^2/m_{B_i}^2$, $y_f = m_f^2/m_T^2$; the Yukawa couplings $C_{i\chi}^{f}$ are

$$
\begin{aligned}
C_{1R}^{f} &= -s_\theta Y_{If}^{u}, \qquad C_{1L}^{f} = -c_\theta Y_{If}^{B'}, \\
C_{2R}^{f} &= c_\theta Y_{If}^{u}, \qquad C_{2L}^{f} = -s_\theta Y_{If}^{B'},
\end{aligned}
\tag{23}
$$

and the denominators are defined by

$$
\begin{aligned}
D_h^a(x,y,z) &= 1 - (1-x)x_1 - y(1-x_1)x_2 - z(x_1 - x_2)x_2, \\
D_h^b(w,x,y,z) &= x_1 + w(1-x_1) - (x - y + 1)x_2 + z x_2^2 + (x - z)x_1 x_2.
\end{aligned}
\tag{24}
$$

The results for the $t \to q\gamma$ decay from each Feynman diagram are obtained as

$$
\begin{aligned}
B_{iL}^{\gamma a} &= -\frac{1}{(4\pi)^2} \int_0^1 dx_1 \int_0^{x_1} dx_2 \frac{1 - x_1}{D_\gamma^a(r_{iH_I^\pm}, r_{it})} C_{iR}^{q} [C_{iR}^{t} r_{it} x_1 + C_{iL}^{t} \sqrt{r_{it}}], \\
B_{iR}^{\gamma a} &= -\frac{1}{(4\pi)^2} \int_0^1 dx_1 \int_0^{x_1} dx_2 \frac{1 - x_1}{D_\gamma^a(r_{iH_I^\pm}, r_{it})} C_{iL}^{q} [C_{iL}^{t} r_{it} x_1 + C_{iR}^{t} \sqrt{r_{it}}], \\
B_{iL}^{\gamma b} &= \frac{Q_b}{(4\pi)^2} \int_0^1 dx_1 \int_0^{x_1} dx_2 \frac{1}{D_\gamma^b(r_{iH_I^\pm}, r_{it})} C_{iR}^{q} [C_{iR}^{t} r_{it} (1-x_1) x_2 + C_{iL}^{t} \sqrt{r_{it}} x_1], \\
B_{iR}^{\gamma b} &= \frac{Q_b}{(4\pi)^2} \int_0^1 dx_1 \int_0^{x_1} dx_2 \frac{1}{D_\gamma^b(r_{iH_I^\pm}, r_{it})} C_{iL}^{q} [C_{iL}^{t} r_{it} (1-x_1) x_2 + C_{iR}^{t} \sqrt{r_{it}} x_1], \\
B_{L}^{\gamma d} &= \frac{Q_t Y_{Iq}^{u} Y_{I3}^{u}}{2(4\pi)^2} y_t \int_0^1 dx_1 \int_0^{x_1} dx_2 x_2 (1-x_1) \left[\frac{1}{D_\gamma^b(y_{H_I}, y_t)} + \frac{1}{D_\gamma^b(y_{A_I}, y_t)} \right],
\end{aligned}
\tag{25}
$$

with

$$
\begin{aligned}
D_\gamma^a(x,y) &= 1 - (1-x)x_1 - y(1-x_1)x_2, \\
D_\gamma^b(x,y) &= x_1 + x(1-x_1) - y(1-x_1)x_2.
\end{aligned}
\tag{26}
$$

It can be seen that C_L^{hc} and $B_L^{\gamma d}$, which arise from Fig. 1(c) and 1(d), are much smaller than other contributions because of the suppression factor $y_t = m_t^2/m_T^2$. To illustrate the smallness of C_L^{hc} and $B_L^{\gamma d}$, we take $m_{H_I} = 65$ GeV, $m_{A_I, H_I^\pm} = 100$ GeV, $m_{B_1, T(B)} = (1, 1.5)$ TeV, $c_\theta = 0.78$, and $Y_{Iq,I3}^{u(B')} = 2$; as a result, $C_{12R}^{hb} \approx 3.2 \times 10^{-3}$, $C_L^{hc} \approx -9.6 \times 10^{-6}$, $B_{1L}^{\gamma a} \approx -1.1 \times 10^{-3}$, and $B_L^{\gamma d} \approx 2.1 \times 10^{-5}$. Hence, the contributions from C_L^{hc} and $B_L^{\gamma d}$ can be neglected.

Using the obtained effective Wilson coefficients, the BRs for $t \to q(h,\gamma)$ can be estimated by the following relations

$$\mathrm{Br}(t \to qh) = \frac{m_t}{32\pi\Gamma_t}\left(1-\frac{m_h^2}{m_t^2}\right)^2(|C_L^h|^2+|C_R^h|^2),$$
$$\mathrm{Br}(t \to q\gamma) = \frac{\alpha m_t}{4\Gamma_t}(|B_L^\gamma|^2+|B_R^\gamma|^2), \quad (27)$$

where Γ_t is the top-quark width. Since the top-quark decay is dominated by the $t \to Wb$ process, for the numerical estimation, we take the next-to-leading order SM result for Γ_t, which is given as [33,34]

$$\Gamma_t = \frac{G_F m_t^3}{8\pi\sqrt{2}}\left(1-\frac{m_W^2}{m_t^2}\right)^2\left(1+2\frac{m_W^2}{m_t^2}\right)\left[1-\frac{2\alpha_s}{3\pi}\left(\frac{2\pi^2}{3}-\frac{5}{2}\right)\right]. \quad (28)$$

B. $t \to qZ$ decay

The $t \to qZ$ decay can arise from Fig. 1(a), 1(b), and 1(d) using Z instead of h/γ. Moreover, the $t \to qZ$ decay can be produced via the ZH_IA_I coupling, where the associated Feynman diagram is shown in Fig. 2.

The decay amplitudes for the $t \to qZ$ decay can be formulated as

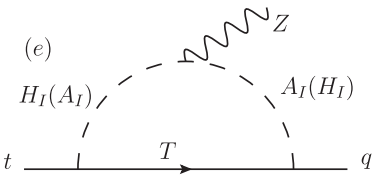

FIG. 2. Feynman diagram mediated by H_I and A_I for the $t \to qZ$ process.

$$\mathcal{L}_{t\to qZ} = \bar{u}_q\gamma_\mu(A_L^Z P_L + A_R^Z P_R)tZ^\mu + \frac{1}{m_t}\bar{u}_q i\sigma_{\mu\nu}k^\nu(B_L^Z P_L + B_R^Z P_R)tZ^\mu. \quad (29)$$

Because of the massive Z boson, the $t \to qZ$ decay involves the vector currents in addition to the tensor currents. Following the Feynman diagrams and using the couplings given in Eqs. (5) and (15)–(17), the effective Wilson coefficients can be summarized as

$$A_\chi^Z = \sum_i\left(A_{i\chi}^{Za} + \sum_j A_{ij\chi}^{Zb}\right) + A_\chi^{Zd} + A_\chi^{Ze},$$
$$B_\chi^Z = \sum_i\left(B_{i\chi}^{Za} + \sum_j B_{ij\chi}^{Zb}\right) + B_\chi^{Zd} + B_\chi^{Ze}. \quad (30)$$

The contributions from each Feynman diagram are shown as

$$A_{iL}^{Za} = -\frac{g(c_W^2-s_W^2)}{2c_W(4\pi)^2}\int_0^1 dx_1\int_0^{x_1} dx_2\frac{1-x_1}{D_h^a(r_{iH_I^\pm}, r_{it}, r_{iZ})}C_{iL}^q(C_{iL}^t r_{it}x_2 + C_{iR}^t\sqrt{r_{it}}),$$
$$B_{iL}^{Za} = -\frac{g(c_W^2-s_W^2)}{2c_W(4\pi)^2}\int_0^1 dx_1\int_0^{x_1} dx_2\frac{1-x_1}{D_h^a(r_{iH_I^\pm}, r_{it}, r_{iZ})}C_{iR}^q(C_{iR}^t r_{it}x_2 + C_{iL}^t\sqrt{r_{it}}),$$
$$X_{ij\chi}^{Zb} = -\frac{gC_{ij}^Z}{c_W(4\pi)^2}\int_0^1 dx_1\int_0^{x_1} dx_2\frac{\tilde{X}_{ij\chi}^Z}{D_h^b(r_{jH_I^\pm}, r_{jt}, r_{ji}, r_{jZ})},$$
$$A_R^{Zd} = -\frac{g(1-2Q_t s_W^2)}{4c_W(4\pi)^2}Y_{Iq}^u Y_{I3}^u\int_0^1 dx_1\int_0^{x_1} dx_2\left(\frac{1+y_Z x_2(x_1-x_2)}{D_h^b(y_{H_I}, y_t, 1, y_Z)} + \frac{1+y_Z x_2(x_1-x_2)}{D_h^b(y_{A_I}, y_t, 1, y_Z)}\right),$$
$$B_L^{Zd} = \frac{g(1-2Q_t s_W^2)}{4c_W(4\pi)^2}y_t Y_{Iq}^u Y_{I3}^u\int_0^1 dx_1\int_0^{x_1} dx_2\left(\frac{x_2(1-x_1)}{D_h^b(y_{H_I}, y_t, 1, y_Z)} + \frac{x_2(1-x_1)}{D_h^b(y_{A_I}, y_t, 1, y_Z)}\right),$$
$$A_R^{Ze} = \frac{gy_t}{4c_W(4\pi)^2}Y_{Iq}^u Y_{I3}^u\int_0^1 dx_1\int_0^{x_1} dx_2\left(\frac{x_2(1-x_1)}{D_Z^e(y_{H_I}, y_{A_I}, y_t, y_Z)} + \frac{x_2(1-x_1)}{D_Z^e(y_{A_I}, y_{H_I}, y_t, y_Z)}\right), \quad (31)$$

$A_{iR}^{Za} = B_{iL}^{Za}$, $B_{iR}^{Za} = A_{iL}^{Za}$, $A_L^{Zd} = B_R^{Zd} = 0$, and $B_L^{Ze} = A_R^{Ze}$ with

$$\tilde{A}_{ijL}^Z = C_{jL}^q[C_{iL}^t(\sqrt{r_{ji}} + r_{jZ}x_2(x_1-x_2)) + C_{iR}^t\sqrt{r_{jt}}(1-x_1)],$$
$$\tilde{A}_{ijR}^Z = C_{jR}^q[C_{iR}^t(\sqrt{r_{ji}} + r_{jZ}x_2(x_1-x_2)) + C_{iL}^t\sqrt{r_{jt}}(1-x_1)],$$
$$\tilde{B}_{ijL}^Z = -C_{jR}^q[C_{iR}^t r_{jt}x_2(1-x_1) + C_{iL}^t(\sqrt{r_{jt}r_{ji}}x_2 + \sqrt{r_{jt}}(x_1-x_2))],$$
$$\tilde{B}_{ijR}^Z = -C_{jL}^q[C_{iL}^t r_{jt}x_2(1-x_1) + C_{iR}^t(\sqrt{r_{jt}r_{ji}}x_2 + \sqrt{r_{jt}}(x_1-x_2))],$$
$$D_Z^e(w,x,y,z) = 1 + (1-x)x_1 - (y-w-x)x_2 + zx_2^2 + yx_1x_2, \quad (32)$$

where $X^{Zb}_{ij\chi}$ and $\tilde{X}^{Z}_{ij\chi}$, which involve the Z flavor-changing couplings, are the contributions from Fig. 1(b). From Eq. (31), it can be seen that A^{Ze}_{R} from Fig. 2 is suppressed by m_t^2/m_T^2. According to earlier analysis, the contribution is small and can be neglected. Moreover, the Z-penguin induced from Fig. 1(d) is comparable with that induced from Fig. 1(b). Using the obtained A^Z_χ and B^Z_χ, the BR for the $t \to qZ$ decay can be written as

$$\begin{aligned}&\mathrm{Br}(t \to qZ)\\ &= \frac{1}{\Gamma_t}\frac{G_F m_t^3}{4\sqrt{2}\pi}\frac{c_W^2}{g^2}\left(1-\frac{m_Z^2}{m_t^2}\right)^2 \sum_{\chi=L,R}\left[|A^Z_\chi + B^Z_{\chi'}|^2\left(1+\frac{2m_Z^2}{m_t^2}\right)\right.\\ &\left. + (|B^Z_{\chi'}|^2 - 2\mathrm{Re}(A^Z_\chi + B^Z_{\chi'})B^{Z*}_{\chi'}))\left(1-\frac{m_Z^2}{m_t^2}\right)\right], \qquad (33)\end{aligned}$$

where $B^Z_{\chi'}$ denotes that when $A^Z_\chi = A^Z_{L(R)}$, $B^Z_{\chi'} = B^Z_{R(L)}$.

IV. CONSTRAINTS

In this section we discuss the possible constraints from the flavor physics, DM data, and oblique parameters.

A. $b \to q'\gamma$ and $\Delta B = 2$

The similar Feynman diagrams for $t \to q\gamma$ can be applied to the $B \to X_{q'}\gamma$ ($q' = d,\ s$) decays, where the current measurements are $\mathrm{BR}(B \to X_s\gamma) = (3.49 \pm 0.19) \times 10^{-4}$ and $\mathrm{BR}(B \to X_d\gamma) = (9.2 \pm 3.0) \times 10^{-6}$ [34]. If there are large effects contributing to the radiative B decays, then the current data may provide a serious bound. From Eq. (5), it can be seen that the involving Yukawa couplings for the $b \to q'\gamma$ decay are $\mathbf{Y}^{B'}_I$ and $\mathbf{Y}^{d}_I$. To understand the influence from $\mathbf{Y}^{B'}_I$ and $\mathbf{Y}^{d}_I$, we write the effective interaction for $b \to q'\gamma$ from the new physics as

$$\begin{aligned}\mathcal{L}_{b\to q'\gamma} &= \frac{G_F V_{tb}V^*_{tq'}}{\sqrt{2}}(C^{\mathrm{NP}}_{7R}\mathcal{O}_{7R} + C^{\mathrm{NP}}_{7L}\mathcal{O}_{7L}),\\ \mathcal{O}_{7\chi} &= \frac{em_b}{4\pi^2}\overline{d_{q'}}\sigma_{\mu\nu}P_\chi b F^{\mu\nu}. \qquad (34)\end{aligned}$$

The $C^{\mathrm{NP}}_{7R,7L}$ mediated by S_I and $H^\pm_I$ can be expressed as

$$\begin{aligned}C^{\mathrm{NP,q'}}_{7R} &= -\frac{\sqrt{2}Y^{B'}_{Iq'}Y^{B'}_{I3}}{G_F V_{tb}V^*_{tq'}}\sum_{i=1}^{2}\frac{Q_b\zeta_i^2}{16m^2_{B_i}}(J(r_{iH_I}) + J(r_{iA_I})),\\ C^{\mathrm{NP,q'}}_{7L} &= -\frac{\sqrt{2}Y^{d}_{Iq'}Y^{d}_{I3}}{G_F V_{tb}V^*_{tq'}}\left[\frac{1}{16m_T^2}(J'(y_{H^\pm_I})Q_t J(y_{H^\pm_I}))\right.\\ &\left. - \sum_{i=1}^{2}\frac{Q_b\xi_i^2}{16m^2_{B_i}}(J(r_{iH_I}) + J(r_{iA_I}))\right],\\ J(a) &= \frac{1-5a-2a^2}{6(1-a)^3} - \frac{a^2\ln a}{2(1-a)^4},\\ J'(a) &= \frac{2+5a-a^2}{12(1-a)^3} + \frac{a\ln a}{2(1-a)^4}, \qquad (35)\end{aligned}$$

with $\zeta_1 = c_\theta$, $\zeta_2 = s_\theta$, $\xi_1 = -s_\theta$, and $\xi_2 = c_\theta$. Using $|V_{ts}| = 0.04$, $|V_{td}| = 0.0088$, $s_\theta = 1/\sqrt{2}$, $\mathbf{Y}^{B'}_I = \mathbf{Y}^d_I = 2$, and $m_{B_1,B_2,T} = (1, 1.5, 1.4)$ TeV, we obtain $C^{\mathrm{NP,s}}_{7R,7L} \sim (-0.051, 0.033)$ and $C^{\mathrm{NP,d}}_{7R,7L} \sim (0.23, -0.15)$, where the SM result is $C^{\mathrm{SM}}_{7R,7L} \sim (-0.3, 0)$ [35]. It can be seen that due to $|V_{td}|/|V_{ts}| \sim 0.22$, the values of $C^{\mathrm{NP,d}}_{7\chi}$ are much larger than those of $C^{\mathrm{NP,s}}_{7\chi}$. Although the value of $C^{\mathrm{NP,d}}_{7R}$ is close to that of C^{SM}_{7R}, the contribution from $\mathcal{O}_{7R}$ operator can be diminished due to the opposite sign in $C^{\mathrm{NP,d}}_{7R}$ and C^{SM}_{7R}; thus, the dominant contribution to $B \to X_d\gamma$ is from $\mathcal{O}_{7L}$. Since $|C^{\mathrm{NP,d}}_{7L}|$ is less than $|C^{\mathrm{SM}}_{7R}|$, $\mathbf{Y}^{B'(d)}_I \sim 2$ are still allowed when the constraint from the $B \to X_d\gamma$ process is taken into account. Hence, $B \to X_{q'}\gamma$ do not provide severe constraints on the parameters $Y^{B'}_{Iq'}$, which are related to the $t \to q(h, V)$ decays.

In addition to the radiative b decays, the Yukawa couplings $\mathbf{Y}^{B'}_I$ and $\mathbf{Y}^d_I$ can also contribute to the $\Delta B = 2$ process through box diagrams mediated by H_I, A_I, and $H^\pm_I$. Since the Yukawa couplings to S_I involves left-handed and right-handed couplings, for simplicity, we write the Yukawa couplings as

$$\mathcal{L}_Y \supset -\eta_{S_I}\bar{B}_i(C^i_{Lf}P_L + C^i_{Rf}P_R)fS_I + \mathrm{H.c.}, \qquad (36)$$

where $\eta_{H_I} = 1$, $\eta_{A_I} = -\sqrt{-1}$, $C^i_{Lf} = \zeta_i Y^{B'}_{If}/\sqrt{2}$, and $C^i_{Lf} = -\xi_i Y^d_{If}/\sqrt{2}$. In order to simplify the expression and show the possible destruction between $\mathbf{Y}^{B'}_I$ and $\mathbf{Y}^d_I$, we take $m_F \equiv m_T \sim m_{B_1} \sim m_{B_2}$ and neglect the small ratios $m^2_{S_I,H^\pm_I}/m^2_{B_1}$; as a result, the effective Lagrangian for $\Delta B = 2$ can be written as

$$\begin{aligned}\mathcal{L}_{\Delta B=2} \sim &-\frac{1}{2(4\pi)^2}\sum_{i,j=1}^{2}\frac{1}{m^2_{B_i}}[C^i_{Lq'}C^i_{L3}C^j_{Lq'}C^j_{L3}(\bar{q}'\gamma_\mu P_L b)^2 + C^i_{Rq'}C^i_{R3}C^j_{Rq'}C^j_{R3}(\bar{q}'\gamma_\mu P_R b)^2\\ &+ (C^i_{Lq'}C^i_{L3}C^j_{Rq'}C^j_{R3} + R \leftrightarrow L)(\bar{q}'\gamma_\mu P_L b)(\bar{q}'\gamma^\mu P_R b)] - \frac{Y^d_{Iq'}Y^d_{I3}}{8(4\pi)^2 m_T^2}(\bar{q}'\gamma_\mu P_R b)^2. \qquad (37)\end{aligned}$$

Using $\sum_i \zeta_i^2 = \sum_i \xi_i^2 = 1$ and the hadronic matrix elements of $B_{q'}$ for various effective operators that were obtained in Ref. [36], the transition matrix element for $B_{q'}$ mixing is obtained as

$$\langle B_{q'}|H_{\rm eff}|\bar{B}_{q'}\rangle \sim \frac{f_{B_{q'}}^2 m_{B_{q'}}}{6(4\pi)^2 m_F^2}\left[((Y_{Iq'}^{B'}Y_{I3}^{B'})^2+\frac{5}{4}(Y_{Iq'}^{d}Y_{I3}^{d})^2)P_1^{\rm VLL} + 2Y_{Iq'}^{B'}Y_{I3}^{B'}Y_{Iq'}^{d}Y_{I3}^{d}P_1^{LR}\right], \tag{38}$$

where P_1^{VLL} and P_1^{LR} are the nonperturbative hadronic effects of $(\bar{q}'\gamma_\mu P_{R(L)}b)^2$ and $(\bar{q}'\gamma_\mu P_L b)(\bar{q}'\gamma^\mu P_R b)$, respectively, and their values are $P_1^{VLL} \approx 0.84$ and $P_1^{LR} \approx -1.62$ [36]. It can be seen that because P_1^{VLL} and P_1^{LR} are opposite in sign, the contributions from $\mathbf{Y}_I^{B'}$ to $\Delta B = 2$ can be diminished by those from $\mathbf{Y}_I^{d}$. To numerically exhibit the cancellation, we take $\hat{w} = Y_{Iq'}^{d}Y_{I3}^{d}$ as a variable, fix $Y_{Iq'}^{B'} = Y_{I3}^{B'} = 2$, and turn Eq. (38) to be a quadratic equation as

$$\frac{5}{4}P_1^{VLL}\hat{w}^2 + 8P_1^{RL}\hat{w} + 16P_1^{VLL} = 0. \tag{39}$$

By solving the quadratic equation, the values of $Y_{Iq'}^{d}Y_{I3}^{d}$, which lead to small $B_{q'}$ mixing, can then be found. Indeed, two solutions to Eq. (39) exist and are obtained as $\hat{w} \approx 1.143$ and $\hat{w} \approx 11.2$. Based on the analysis, it is known that the strict constraint from the $\Delta B = 2$ process can be avoided when the left-handed and right-handed current couplings are simultaneously considered.

B. Oblique parameters

Since the Z_2-odd quark B in doublet Q_4 mixes with the singlet B', the mixing effect leads to the mass difference between T and B. In Eq. (4), it can be seen that the mass splitting within the vectorlike quark doublet can be expressed as $\delta m_{Q_4} = |m_T - m_{B_2}|$ and is dictated by $v y_{B'}/\sqrt{2}$. This mass splitting contributes to the electroweak oblique parameters, where the current measurements with $U = 0$ are given as [34]

$$S = 0.02 \pm 0.07, \qquad T = 0.06 \pm 0.06. \tag{40}$$

Therefore, the precision measurements of electroweak oblique parameters [37] may constrain $y_{B'}$ or the mixing angle θ. Take the constraints into account, following the results in [38,39], we write the oblique correction to the T parameter as

$$\Delta T_{Q_4} = \frac{N_c}{8\pi s_W^2 c_W^2}[s_\theta^2\Theta_{+-}(z_T, z_{B_1}) + c_\theta^2\Theta_{+-}(z_T, z_{B_2}) - s_\theta^2 c_\theta^2\Theta_{+-}(z_{B_1}, z_{B_2})], \tag{41}$$

where $N_c = 3$ is the color number, $z_f = m_f^2/m_Z^2$, and $\Theta_{+-}(a,b) = \theta_+(a,b) + \theta_-(a,b)$, with

$$\theta_+(a,b) = a + b - \frac{2ab}{a-b}\ln\left(\frac{a}{b}\right),$$
$$\theta_-(a,b) = 2\sqrt{ab}\left(\frac{a+b}{a-b}\ln\left(\frac{a}{b}\right) - 2\right). \tag{42}$$

When $y_{B'} = 0$, it can be seen that $s_\theta = 0$ and $m_T = m_{B_2} = m_{4Q}$. Due to $\theta_\pm(a,a) = 0$, we obtain $\Delta T = 0$.

The correction to the S parameter can be expressed as

$$\Delta S_{Q_4} = \frac{N_c}{\pi}[s_\theta^2\Psi_{+-}(z_T, z_{B_1}) + c_\theta^2\Psi_{+-}(z_T, z_{B_2}) - s_\theta^2 c_\theta^2\chi_{+-}(z_{B_1}, z_{B_2})], \tag{43}$$

where $\Psi_{+-}(a,b) = \Psi_+(a,b) + \Psi_-(a,b)$ and $\chi_{+-}(a,b) = \chi_+(a,b) + \chi_-(a,b)$, with

$$\Psi(a,b) = \frac{1}{3} - \frac{1}{9}\ln\left(\frac{a}{b}\right), \quad \Psi_-(a,b) = -\frac{a+b}{6\sqrt{ab}},$$
$$\chi_+(a,b) = \frac{5(a^2+b^2)-22ab}{9(a-b)^2} + \frac{3ab(a+b)-a^3-b^3}{3(a-b)^3}\ln\left(\frac{a}{b}\right),$$
$$\chi_-(a,b) = -\sqrt{ab}\left[\frac{a+b}{6ab} - \frac{a+b}{(a-b)^2} + \frac{2ab}{(a-b)^3}\ln\left(\frac{a}{b}\right)\right]. \tag{44}$$

Similar to ΔT_{Q_4}, when $y_{B'} = 0$, due to $\Psi_{+-}(a,a) = 0$ and $\chi_\pm(a,a) = 0$, we obtain $\Delta S_{Q_4} = 0$. With $c_\theta = 0.8$, $\Delta S_{Q_4} \sim 0.01$, which is much smaller than ΔT_{Q_4}. Thus, we only take the T parameter as the potential constraint.

The mass splittings among $H_I^\pm$, H_I, and A_I also contribute to the T parameter. Following the results shown in [30], the correction of the inert Higgs doublet to the T parameter is expressed as

$$\Delta T_{\Phi_I} = \frac{1}{16\pi s_W^2 c_W^2}(\theta_+(z_{H_I^\pm}, z_{H_I}) + \theta_+(z_{H_I^\pm}, z_{A_I}) - \theta_+(z_{H_I}, z_{A_I})). \tag{45}$$

C. Higgs production and $h \to \gamma\gamma$

From Eqs. (6) and (9), the SM Higgs has extra couplings to $H_I^\pm$ and B_i, where the former can induce the $h\gamma\gamma$ effective coupling, and the latter can generate $h\gamma\gamma$ and hgg effective couplings. With the precision measurements for the Higgs production and Higgs decay to diphoton, the new physics effect could be strictly bounded. To show the new physics effect, the signal strength for $pp \to h \to \gamma\gamma$ is defined as

$$\mu_{\gamma\gamma} = \frac{\sigma(pp \to h)}{\sigma(pp \to h)^{\rm SM}} \frac{\mathrm{BR}(h \to \gamma\gamma)}{\mathrm{BR}(h \to \gamma\gamma)^{\rm SM}}, \tag{46}$$

where the measurements from ATLAS and CMS at $\sqrt{s} = 13$ TeV are given as 1.10 ± 0.10 using 139 fb^{-1} [40] and $1.03^{+0.11}_{-0.09}$ using 137 fb^{-1} [41], respectively.

The loop-induced effective interactions for $h\gamma\gamma$ and hgg can be parameterized as

$$\mathcal{L}_{hVV} = \frac{\alpha}{4\pi}\frac{a_{\gamma\gamma}}{m_h} h F_{\mu\nu}F^{\mu\nu} + \frac{\alpha_s}{4\pi}\frac{a_{gg}}{m_h} h G^a_{\mu\nu}G^{a\mu\nu}, \tag{47}$$

where the Feynman diagrams mediated by $H_I^\pm$ and B_i are shown in Fig. 3. The resulting $a_{\gamma\gamma}$ and a_{gg} in the model are obtained as

$$\begin{aligned} a_{\gamma\gamma} &= \frac{g m_h}{2 m_W}\left(a_{2\gamma}^{\rm SM} + \frac{\lambda_3 v m_W}{g m_{H_I^\pm}^2} F_0(\tau_{H_I^\pm}) \right. \\ &\quad \left. + N_c Q_b^2 \sum_i \frac{y_{ii}^h v}{\sqrt{2} m_t} F_{1/2}(\tau_{B_i}) \right), \\ a_{gg} &= \frac{g m_h}{4 m_W}\left(a_{2g}^{\rm SM} + \sum_i \frac{y_{ii}^h v}{\sqrt{2} m_t} F_{1/2}(\tau_{B_i}) \right), \end{aligned} \tag{48}$$

where $a_{2\gamma}^{\rm SM} \approx 6.51 - i0.02$ and $a_{2g}^{\rm SM} \approx -0.69$ are the SM results; $y_{11}^h = -s_{2\theta} y_{B'}$ and $y_{22}^h = s_{2\theta} y_{B'}$, and the functions F_0 and $F_{1/2}$ are given as

$$\begin{aligned} F_0(\tau) &= \tau(1 - \tau f(\tau)), \\ F_{1/2}(\tau) &= -2\tau(1 + (1-\tau) f(\tau)), \end{aligned} \tag{49}$$

with $\tau = 4m_f^2/m_h^2$ and $f(\tau) = (\arcsin(1/\sqrt{\tau}))^2$. Considering that we focus on the case with $2m_{H_I^\pm}, 2m_{B_i} > m_h$, the on-shell condition in the loop propagators is not available.

When $m_{B_i} \gg m_h$, $F_{1/2}(\tau) \to -4/3$. Because $y_{11}^h = -y_{22}^h$, the contributions to the hgg effective coupling from the B_1 and B_2 quarks are canceled each other; that is, the Higgs production through the gluon-gluon fusion is the same as the SM. Thus, the signal strength for $pp \to h \to \gamma\gamma$ can be simplified as

$$\mu_{\gamma\gamma} \approx \frac{\mathrm{BR}(h \to \gamma\gamma)}{\mathrm{BR}(h \to \gamma\gamma)^{\rm SM}} \approx \left| 1 + \frac{\lambda_3 v m_W}{g m_{H_I}^2 a_{2\gamma}^{\rm SM}} F_0(\tau_{H_I^\pm}) \right|^2, \tag{50}$$

where the new physics on the Higgs width Γ_h is assumed to be small and neglected in $\mu_{\gamma\gamma}$. To suppress the invisible Higgs decay $h \to S_I S_I$ and to have $\Gamma_h \approx \Gamma_h^{\rm SM}$, we simply take $m_h < 2m_{S_I}$ in the model. Using $m_{H_I^\pm} = 100$ GeV, the $H_I^\pm$ effect on $\mu_{\gamma\gamma}$ can be estimated as $-0.197\lambda_3$. If we take the allowed range of $\mu_{\gamma\gamma}$ to be $0.8 < \mu_{\gamma\gamma} < 1.2$, then λ_3 is limited to be $\lambda_3 < 0.5$. Hence, the λ_3 parameter can be bounded by the $h \to \gamma\gamma$ measurement.

D. DM direct detection

In the inert Higgs doublet model, although there is no ZH_IH_I coupling at the tree level, the nonvanishing ZH_IA_I coupling will contribute to the DM-nucleon scattering. To satisfy the DM direct detection experiments, the Z-mediated $H_I n \to A_I n$ process has to be suppressed, where n denotes the nucleon. The process can be kinematically forbidden by requiring $m_{A_I} - m_{H_I}$ to be larger than the kinetic energy of the DM, where the typical energy is tens of keV. In the study, we take $m_{A_I} - m_{H_I} > 1$ GeV.

The spin-independent (SI) DM-nucleon scattering can occur via the trilinear coupling hH_IH_I shown in Eq. (9). The Higgs-mediated cross section can be formulated as [30]

$$\sigma_h^{\rm SI} = \frac{\mu_{H_I n}^2}{4\pi}\left| \frac{\lambda_L}{m_{H_I} m_h^2} \right|^2 f_n^2 m_n^2, \tag{51}$$

where $\mu_{H_I n} = m_{H_I} m_n/(m_{H_I} + m_n)$ is the DM-nucleon reduced mass, and $f_n \approx 0.3$ is the nucleon matrix element. With $m_n = 0.94$ GeV and $m_{H_I} = 70$ GeV, we have

$$\sigma_h^{\rm SI} \approx 2.0 \times 10^{-42}(\lambda_3 - |\lambda_4| - |\lambda_5|)^2 \ \mathrm{cm}^2. \tag{52}$$

To satisfy the XENON1T upper limit of 7×10^{-47} cm^2 [42], $\lambda_3 - |\lambda_4| - |\lambda_5| < 5 \times 10^{-3}$ is required; that is, $\lambda_3 \sim |\lambda_4| + |\lambda_5|$. As mentioned earlier, λ_3 is bounded by $\mu_{\gamma\gamma}$. Therefore, the magnitude $|\lambda_4|$ can be bounded by the DM direct detection. With the mass ordering of $m_{H_I^\pm} > m_{A_I} > m_{H_I}$, we obtain $|\lambda_5| < |\lambda_4|$.

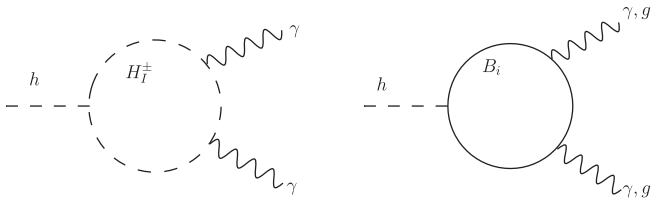

FIG. 3. Feynman diagram for $h \to (\gamma\gamma, gg)$ induced by $H_I^\pm$ and B_i.

V. NUMERICAL ANALYSIS AND DISCUSSIONS

Many free parameters are involved in the phenomenological analysis, such as Yukawa couplings $\mathbf{Y}_I^u$ and $\mathbf{Y}_I^{B'}$, the inert scalar masses $m_{H_I, A_I, H_I^\pm}$, the Z_2-odd quark masses $m_{B_1, B_2, T}$, and the parameter λ_3 in the scalar potential. Before discussing their influence on the rare top decays, we first determine the allowed ranges for the free parameters and then use the constrained parameter values to analyze the implications on the rare top decays. For the

numerical analysis, the current experimental upper limits are taken as [34]

$$\begin{aligned} \mathrm{BR}(t \to q\gamma) &< 1.8 \times 10^{-4}, \\ \mathrm{BR}(t \to qZ) &< 5 \times 10^{-4}, \\ \mathrm{BR}(t \to uh) &< 1.2 \times 10^{-3}, \\ \mathrm{BR}(t \to ch) &< 1.1 \times 10^{-3}. \end{aligned} \tag{53}$$

A. Parameter choices and constraints

As stated earlier, the radiative B decay cannot severely bound the Yukawa couplings. Thus, we employ the perturbative unitarity constraint, and the upper limits of the Yukawa couplings are required to be $|\mathbf{Y}_I^{u(B')}| < 2\sqrt{2\pi}$ [43]. To obtain the mass upper limit of the Z_2-odd quarks, we apply the similar constraints for the stop and sbottom with the R-parity conserving supersymmetry, where using the data with an integrated luminosity of 139 fb^{-1} at $\sqrt{s} = 13$ TeV [44], the mass below 1 TeV has been excluded by ATLAS when the neutralino mass is below 100 GeV. Thus, for the parameter scan, we assume $m_{B_1} < m_{B_2}$ and take the mass regions for $m_{B_{1,2}}$ and m_T to be

$$m_{B_1} \in (1000, 1200)\ \mathrm{GeV}, \quad m_{B_2,T} \in (1000, 2000)\ \mathrm{GeV}. \tag{54}$$

If H_I is the DM candidate in the inert Higgs model, then $m_{H_I} \sim m_W$ can fit the observed DM relic abundance [30]. It has been studied that the direct bounds from colliders on m_{H_I,A_I} are not strict, and the bound on $m_{H_I^\pm}$, which converts from the SUSY search at LEP, is $m_{H_I^\pm} >$ 70–90 GeV [45–48]. Therefore, the mass regions of H_I, A_I, and $H_I^\pm$ are taken as

$$m_{H_I,A_I,H_I^\pm} \in (70, 120)\ \mathrm{GeV}. \tag{55}$$

The mass regions in Eqs. (54) and (55) are only used to set the boundaries of the scanned parameters. Their mass differences are dictated by the oblique T parameters, as shown in Eqs. (41) and (45). To understand the T-parameter constraints, we perform the parameter scan based on the chosen parameter regions. The correlation of $m_{B_2} - m_T$ and $m_{B_2} - m_{B_1}$ is shown in Fig. 4(a), where 5×10^6 random sampling points are used. The allowed region for $m_{B_2} - m_T$ is limited within 200 GeV and that for $m_{B_2} - m_{B_1}$ is wider; that is, the mass splitting in the same representation is strictly constrained. Therefore, it is appropriate if we take $m_{B_2} - m_T = 100$ GeV for the top decay analysis. Similarly, the T-parameter constraint on $m_{A_I} - m_{H_I}$ and $m_{H_I^\pm - H_I}$ is shown in Fig. 4(b), where the mass ordering $m_{H^\pm} > m_{A_I} > m_{H_I}$ is applied. Because the chosen ranges of $m_{H_I,A_I,H_I^\pm}$ in Eq. (55) are not broad, the constraint is not significant. As $m_{B_2} - m_T$ is related to the parameter $y_{B'}$ or s_θ, the correlation between $y_{B'}$ and s_θ under the

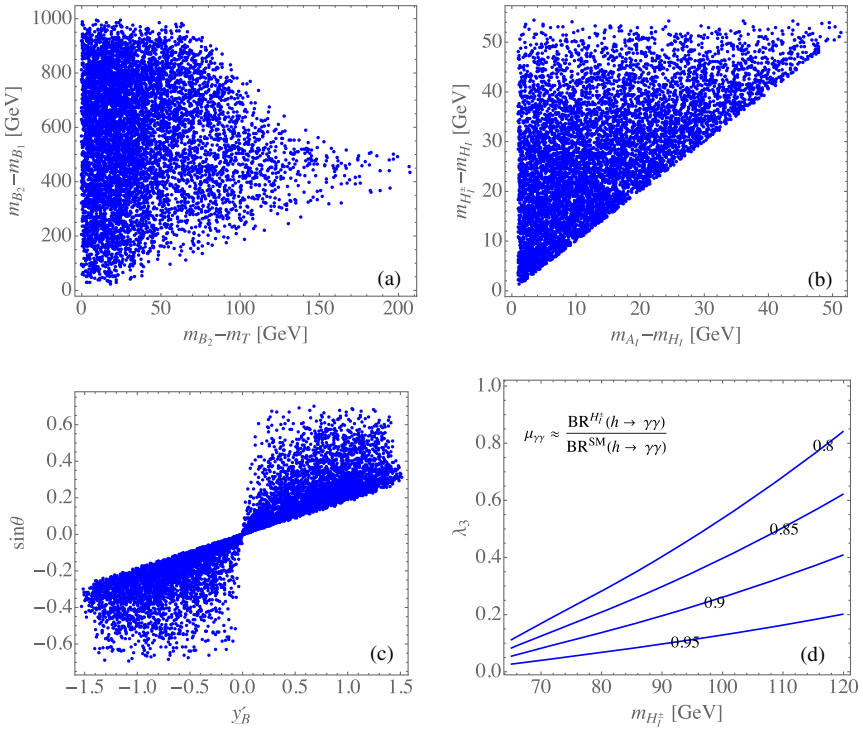

FIG. 4. Plots (a)–(c) show the constraints from the oblique T-parameter, and plot (d) is the constraint from $\mu_{\gamma\gamma}$.

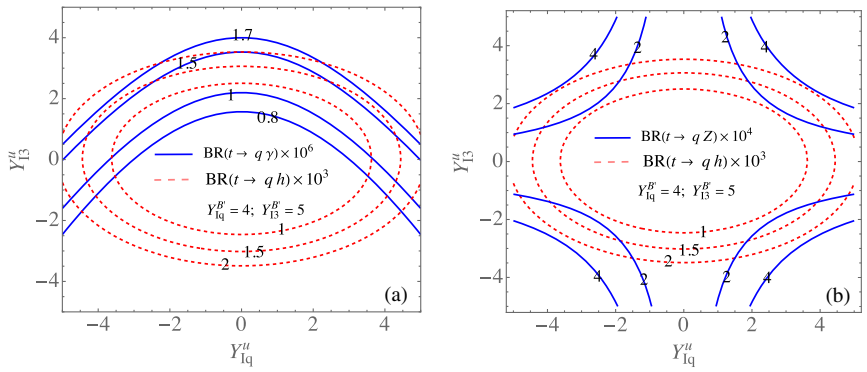

FIG. 5. Contours for (a) $\mathrm{BR}(t \to q\gamma)$ and (b) $\mathrm{BR}(t \to qZ)$ as a function of Y^u_{Iq} and Y^u_{I3}, where the dashed lines are $\mathrm{BR}(t \to qh)$ and $Y^{B'}_{Iq,I3} = (4, 5)$ are used. The other taken parameter values can be found in the text.

T-parameter constraint is shown in Fig. 4(c). When $m_{B_2} - m_T$ is limited, the allowed $y_{B'}$ parameter is bounded by $|y'_B| \lesssim 1.5$, where the maximum s_θ can still reach $|s_\theta|_{\max} \sim 1/\sqrt{2}$. Using Eq. (50), the strength signal for the Higgs to diphoton as a function of $m_{H_I^\pm}$ and λ_3 is shown in Fig. 4(d). If the uncertainty of the observed strength signal is 10% of the SM result, then the λ_3 value is limited to be approximately 0.2 when $m_{H^\pm} = 90$ GeV is used.

B. BRs for $t \to q(h,\gamma)$ and $t \to qZ$

After analyzing the constraints of the parameters, in this subsection, we numerically calculate and discuss the S_I- and $H_I^\pm$-mediated contributions to the $t \to q(h, \gamma)$ and $t \to qZ$ decays. As stated before, many parameters are involved in the processes. We can use the parameter scan to comprehend the influence of various parameters. Before scanning the parameters, we need to examine whether the $t \to qV$ and $t \to qh$ decays can be simultaneously enhanced to the current experimental upper limits.

For the purpose of illustration, we use the formulas given in Eqs. (27) and (33) and show the contours for $\mathrm{BR}(t \to q\gamma)$ (in units of 10^{-6}) and $\mathrm{BR}(t \to qZ)$ (in units of 10^{-4}) in Figs. 5(a) and 5(b), respectively, where the dashed lines denote $\mathrm{BR}(t \to qh)$. The parameter values are taken as $m_{H_I, A_I, H_I^\pm} = (65, 70, 90)$ GeV, $m_{B_1,B_2,T} = (1, 1.5, 1.4)$ TeV, $\lambda_3 = 0.2$, $y_{B'} = 1.0$, and $Y^{B'}_{Iq,I3} = (4, 5)$. As shown in the plots, the BRs for $t \to q(h, \gamma, Z)$ with the chosen parameter values can reach the levels of $(10^{-3}, 10^{-6}, 10^{-4})$, where with the exception of $t \to q\gamma$, $t \to q(h, Z)$ can reach the current upper bounds that are shown in Eq. (53). Based on the results, although the used Yukawa couplings are lower than the upper limit from the perturbative unitarity, $\mathrm{BR}(t \to q\gamma)$ of $O(10^{-6})$ inevitably has to reply on the large Yukawa couplings. To illustrate the situation with small Yukawa couplings, we fix $Y^{B'}_{Iq,I3} = (2, 3)$ and show the regions for $\mathrm{BR}(t \to qh) \geq 1.5 \times 10^{-4}$ and $\mathrm{BR}(t \to qZ) \geq 1.5 \times 10^{-5}$ as a function of $Y^u_{Iq,I3}$ in Fig. 6. In these chosen regions, $\mathrm{BR}(t \to q\gamma)$ is far below 10^{-6}.

In the following, we discuss the influence of various parameters on the rare top decays in detail. To reduce the number of scanned parameters, the parameters that are insensitive to the studying phenomena are fixed as follows:

$$m_{H_I, A_I, H_I^\pm} = (65, 70, 90)\ \text{GeV}, \qquad \lambda_3 = 0.2, \quad (56)$$

where the values are chosen to satisfy the constraints obtained earlier. Thus, the involving parameters are the Z_2-odd quark masses $m_{B_1,B_2,T}$ and Yukawa couplings $y_{B'}$, $Y^{B',u}_{I1,I3}$, and their scanning regions are chosen as

$$m_{B_1} \in [1000, 1300]\ \text{GeV}, \qquad m_T \in [1000, 2000]\ \text{GeV},$$
$$m_{B_2} = m_T + 100,$$
$$y_{B'} \in (-1.5, 1.5), \quad Y^{B'}_{Iq,I3} \in (-3, 3), \quad Y^u_{Iq,I3} \in (-3, 3). \quad (57)$$

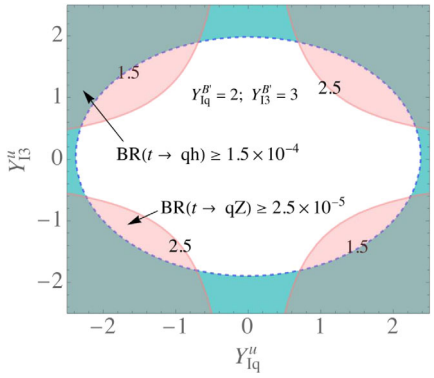

FIG. 6. Regions for $\mathrm{BR}(t \to qh) \geq 1.5 \times 10^{-4}$ and $\mathrm{BR}(t \to qZ) \geq 1.5 \times 10^{-5}$ as a function for Y^u_{Iq} and Y^u_{I3}, where $Y^{B'}_{Iq} = 2$, and $Y^{B'}_{I3} = 3$ are used.

According to the ATLAS results of $\mathrm{BR}(t \to ug) \lesssim 0.61 \times 10^{-4}$ [27], we can indirectly bound the $t \to q\gamma$ to be $\mathrm{BR}(t \to q\gamma) \lesssim 3.2 \times 10^{-6}$ using $\mathrm{BR}(t \to q\gamma) \sim \mathrm{BR}(t \to qg)\alpha/(C_F\alpha_s)$ in the model, where the upper limit is smaller than the current experimental upper limit. Therefore, it is sufficient to use the small Yukawa couplings for the scan. In addition, in order to show the resulting BRs that can reach the sensitivities at the HL LHC, we require the obtained BRs for the rare top decays to be

$$10^{-5} < \mathrm{BR}(t \to qh) < 10^{-3},$$
$$2 \times 10^{-5} < \mathrm{BR}(t \to qZ) < 5 \times 10^{-4}. \quad (58)$$

However, the radiative top decay is required to be $\mathrm{BR}(t \to q\gamma) > 0.3 \times 10^{-6}$. Since we have taken small Yukawa couplings, $\mathrm{BR}(t \to q\gamma)$ cannot reach the current upper limit, i.e., $O(10^{-4})$. Thus, it is not necessary to set the upper value for $\mathrm{BR}(t \to q\gamma)$.

We show the scatter plots for the Yukawa couplings of $Y^{B'}_{Iq,I3}$ and $Y^{u}_{Iq,I3}$, which fit the ranges given in Eqs. (57) and (58), in Figs. 7(a) and 7(b). Hence, $|Y^{B',u}_{Iq,I3}| < 1$ are disfavored. The correlation between $y_{B'}$ and m_{B_1} is shown in Fig. 7(c). From the numerical results, $|y_{B'}| \lesssim 0.5$ is excluded. In addition, the correlation between m_{B_1} and m_{B_2} can be found in Fig. 7(d).

After knowing the constrained parameter ranges, in the following, we discuss the implications on the $t \to q(\gamma, h, Z)$ decays. Because $t \to q\gamma$ and $t \to qh$ have similar chirality structures in decay amplitudes and arise from the similar Feynman diagrams, we analyze their numerical results together. When neglecting the small contributions from Figs. 1(c) and 1(d), as stated earlier, $t \to q\gamma, qh$ decays can arise from Figs. 1(a) and 1(b). Compared to the $H^{\pm}\gamma$ coupling, the $B_iB_i\gamma$ coupling has a suppression factor from the electric charge of B_i; thus, the $t \to q\gamma$ decay indeed is dominated by Fig. 1(a). By contrast, because the $H^{\pm}_I h$ coupling is λ_3 and is limited by the $h \to \gamma\gamma$ measurement, the dominant contribution to $t \to qh$ is from Fig. 1(b). Hence, the resulting $\mathrm{BR}(t \to q\gamma)$ and $\mathrm{BR}(t \to qh)$ as a function of m_{B_1} are shown in Figs. 8(a) and 8(b). In the chosen Yukawa couplings, the BR for $t \to q\gamma$ can only maximally reach of the $O(10^{-7})$, which is consistent with the indirect bound from the $t \to qg$ measurement. The dependence of $B(t \to qh)$ with respect to m_{B_2} is shown in Fig. 8(c), where $\mathrm{BR}(t \to qh)$ increases as m_{B_2} increases. The reason for the behavior can be understood as the relaxed cancellation between B_1 and B_2 when the mass of B_2 increases; that is, the B_1 becomes the dominant effect if $m_{B_2} \gg m_{B_1}$. In Fig. 8(d), we show the scatter plot for the correlation between $\mathrm{BR}(t \to q\gamma)$ and $\mathrm{BR}(t \to qh)$. The dashed lines in Fig. 8 denote the sensitivity of the HL LHC.

In addition to the dipole operators, unlike the $t \to q\gamma$ decay, $t \to qZ$ also involves the vectorial types of operators in the decay amplitude, which are not associated with the chirality flip in the quark currents, so they are the dominant

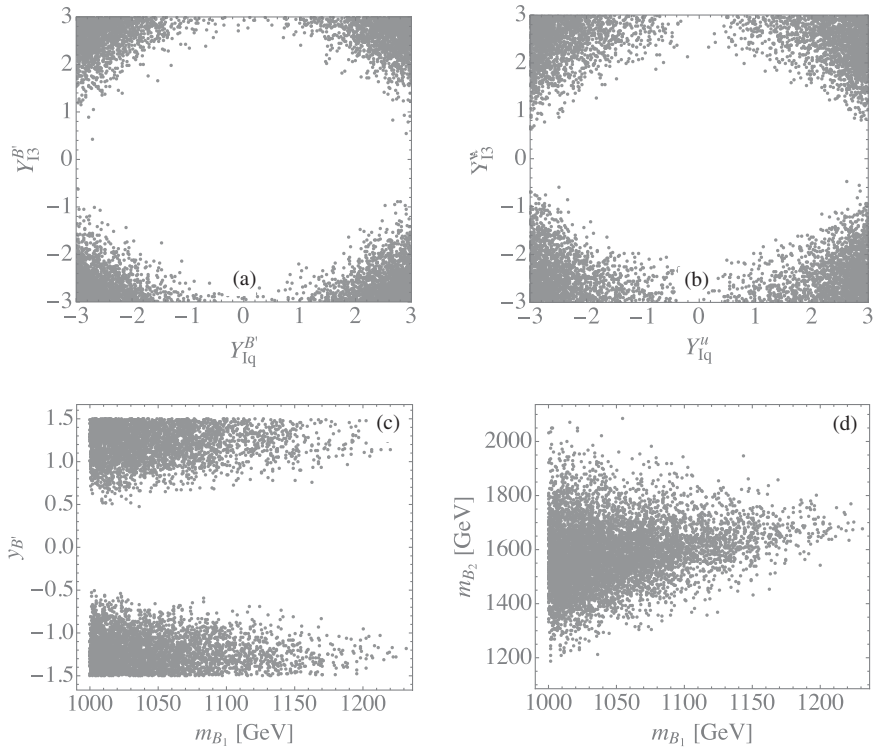

FIG. 7. Correlations of Yukawa couplings and $m_{B_{1,2}}$ that fit the taken ranges shown in Eqs. (57) and (58).

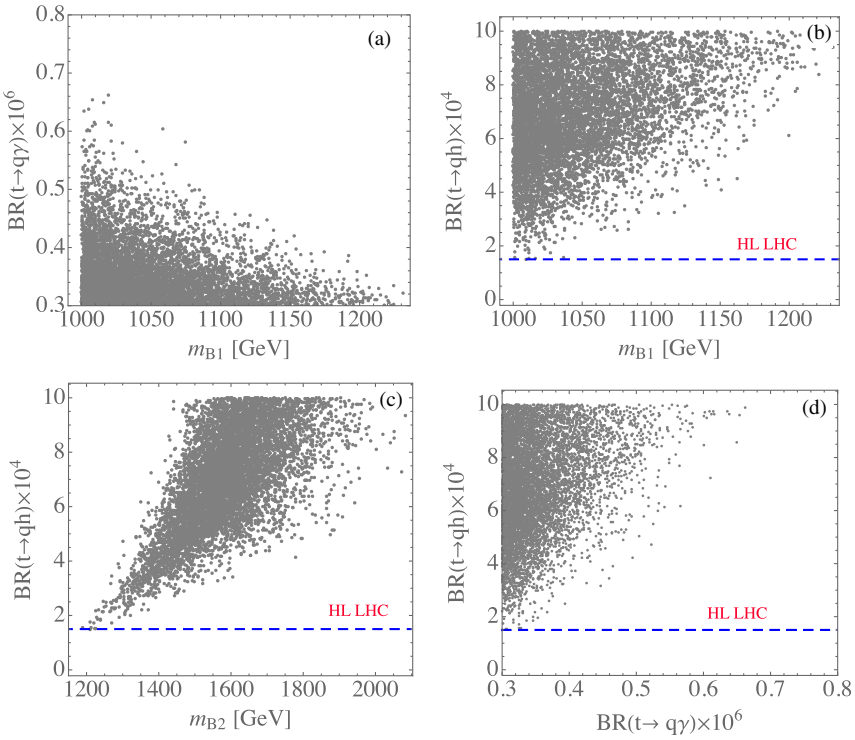

FIG. 8. (a)–(b) $\mathrm{BR}(t \to q\gamma, qh)$ as a function of m_{B_1}; (c) $\mathrm{BR}(t \to qh)$ as a function of m_{B_2}, and (d) correlation between $\mathrm{BR}(t \to q\gamma)$ and $\mathrm{BR}(t \to qh)$.

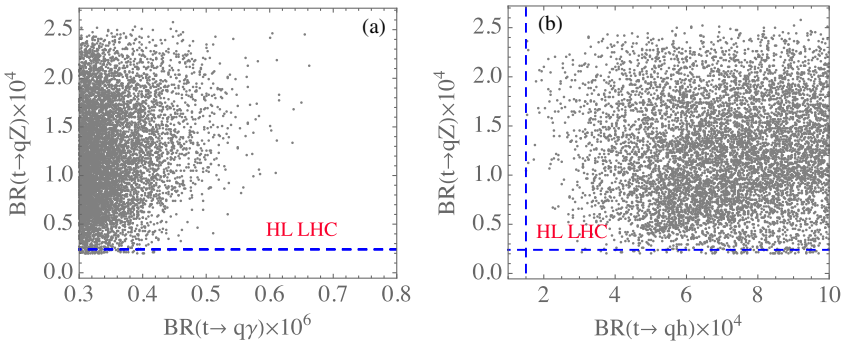

FIG. 9. Correlation of $\mathrm{BR}(t \to qZ)$ with (a) $\mathrm{BR}(t \to q\gamma)$ and (b) $\mathrm{BR}(t \to qh)$.

effect. To observe the influence of the new physics effects on $t \to qZ$, we show the scatter plots for the correlations of $\mathrm{BR}(t \to qZ)$ with $\mathrm{BR}(t \to q\gamma)$ and with $\mathrm{BR}(t \to qh)$ in Figs. 9(a) and 9(b), respectively, where the dashed lines are the sensitivity that the HL LHC is planning to reach. With the exception of the $t \to q\gamma$ decay, the BRs for the $t \to qh$ and $t \to qZ$ decays in the model can reach the level of $O(10^{-4})$.

VI. SUMMARY

In this study, we investigated the potential effects that can enhance the top-FCNC processes, where the processes are highly suppressed in the SM. If we assume that $t \to qh$ and $t \to qZ$ are induced via quantum loop diagrams, the intermediate states in the loop may have different properties from the SM particles. Inspired from the mechanism of the scotogenic neutrino mass, we consider that the new particles carry an extra Z_2-odd parity, whereas the SM particles are Z_2-even.

To retain the basic element in the radiative neutrino mass [28], in addition to the Z_2 discrete symmetry, we can extend the SM by including one inert Higgs doublet, one vectorlike Z_2-odd doublet quark, and one vectorlike Z_2-odd singlet quark.

The potential constraints from the experimental observations are taken into account, such as the oblique parameters, Higgs to diphoton decay, and DM direct detection. Although the $b \to s\gamma$ decay and $\Delta B = 2$ process can be induced in the model, their effects can be small.

According to the recent ATLAS's measurement that shows $\mathrm{BR}(t \to qg) \lesssim O(10^{-4})$, we found that the indirect bound on $t \to q\gamma$ in the model is $\mathrm{BR}(t \to q\gamma) \lesssim 3.2 \times 10^{-6}$, which is lower than the expected sensitivity at the HL LHC. With the exception of $t \to q\gamma$, the branching ratios for the loop-induced $t \to qh$ and $t \to qZ$ decays in the model can be of the order of 10^{-4} and can be tested at the HL LHC.

ACKNOWLEDGMENTS

This work was supported in part by the Ministry of Science and Technology, Taiwan under the Grant No. MOST-110-2112-M-006-010-MY2 (C. H. Chen). The work was supported in part by the Fundamental Research Funds for the Central Universities (T. N.).

[1] S. L. Glashow, J. Iliopoulos, and L. Maiani, Phys. Rev. D **2**, 1285 (1970).
[2] J. A. Aguilar-Saavedra, Acta Phys. Pol. B **35**, 2695 (2004).
[3] G. Abbas, A. Celis, X. Q. Li, J. Lu, and A. Pich, J. High Energy Phys. 06 (2015) 005.
[4] S. Balaji, Phys. Rev. D **102**, 113010 (2020).
[5] ATLAS Collaboration, Report No. ATL-PHYS-PUB-2019-001, CERN.
[6] ATLAS Collaboration, Report No. ATL-PHYS-PUB-2016-019, CERN.
[7] CMS Collaboration, Report No. CERN-LHCC-2017-023, CERN.
[8] K. J. Abraham, K. Whisnant, J. M. Yang, and B. L. Young, Phys. Rev. D **63**, 034011 (2001).
[9] G. Eilam, A. Gemintern, T. Han, J. M. Yang, and X. Zhang, Phys. Lett. B **510**, 227 (2001).
[10] J. A. Aguilar-Saavedra, Phys. Rev. D **67**, 035003 (2003); **69**, 099901(E) (2004).
[11] U. K. Dey and T. Jha, Phys. Rev. D **94**, 056011 (2016).
[12] R. Gaitan, R. Martinez, J. H. M. de Oca, and E. A. Garces, Phys. Rev. D **98**, 035031 (2018).
[13] M. Badziak and K. Harigaya, Phys. Rev. Lett. **120**, 211803 (2018).
[14] J. F. Shen, Y. Q. Li, and Y. B. Liu, Phys. Lett. B **776**, 391 (2018).
[15] C. W. Chiang, U. K. Dey, and T. Jha, Eur. Phys. J. Plus **134**, 210 (2019).
[16] K. Y. Oyulmaz, A. Senol, H. Denizli, A. Yilmaz, I. Turk Cakir, and O. Cakir, Eur. Phys. J. C **79**, 83 (2019).
[17] C. H. Chen and T. Nomura, Eur. Phys. J. C **79**, 644 (2019).
[18] M. A. Arroyo-Ureña, R. Gaitán, E. A. Herrera-Chacón, J. H. Montes de Oca Y., and T. A. Valencia-Pérez, J. High Energy Phys. 07 (2019) 041.
[19] L. Shi and C. Zhang, Chin. Phys. C **43**, 113104 (2019).
[20] Y. B. Liu and S. Moretti, Phys. Rev. D **101**, 075029 (2020).
[21] W. S. Hou, T. H. Hsu, and T. Modak, Phys. Rev. D **102**, 055006 (2020).
[22] S. Y. Bie, G. L. Liu, and W. Wang, Chin. Phys. C **45**, 013106 (2021).
[23] P. Gutierrez, R. Jain, and C. Kao, Phys. Rev. D **103**, 115020 (2021).
[24] Y. Liu, B. Yan, and R. Zhang, Phys. Lett. B **827**, 136964 (2022).
[25] F. M. Cai, S. Funatsu, X. Q. Li, and Y. D. Yang, Eur. Phys. J. C **82**, 881 (2022).
[26] A. I. Hernández-Juárez and G. Tavares-Velasco, arXiv:2203.16819.
[27] G. Aad *et al.* (ATLAS Collaboration), Eur. Phys. J. C **82**, 334 (2022).
[28] E. Ma, Phys. Rev. D **73**, 077301 (2006).
[29] N. Aghanim *et al.* (Planck Collaboration), Astron. Astrophys. **641**, A6 (2020); **652**, C4(E) (2021).
[30] R. Barbieri, L. J. Hall, and V. S. Rychkov, Phys. Rev. D **74**, 015007 (2006).
[31] K. G. Klimenko, Theor. Math. Phys. **62**, 58 (1985).
[32] K. Kannike, Eur. Phys. J. C **72**, 2093 (2012).
[33] M. Jezabek and J. H. Kuhn, Nucl. Phys. **B314**, 1 (1989).
[34] P. A. Zyla *et al.* (Particle Data Group), Prog. Theor. Exp. Phys. **2020**, 083C01 (2020).
[35] G. Buchalla, A. J. Buras, and M. E. Lautenbacher, Rev. Mod. Phys. **68**, 1125 (1996).
[36] A. J. Buras, S. Jager, and J. Urban, Nucl. Phys. **B605**, 600 (2001).
[37] M. E. Peskin and T. Takeuchi, Phys. Rev. D **46**, 381 (1992).
[38] L. Lavoura and J. P. Silva, Phys. Rev. D **47**, 2046 (1993).
[39] C. Y. Chen, S. Dawson, and E. Furlan, Phys. Rev. D **96**, 015006 (2017).
[40] ATLAS Collaboration, Report No. ATLAS-CONF-2020-026, CERN.
[41] CMS Collaboration, Report No. CMS-PAS-HIG-19-015, CERN.
[42] E. Aprile *et al.* (XENON Collaboration), Phys. Rev. Lett. **121**, 111302 (2018).
[43] A. Castillo, R. A. Diaz, and J. Morales, Int. J. Mod. Phys. A **29**, 1450085 (2014).
[44] G. Aad *et al.* (ATLAS Collaboration), J. High Energy Phys. 04 (2021) 165.
[45] A. Pierce and J. Thaler, J. High Energy Phys. 08 (2007) 026.
[46] E. Lundstrom, M. Gustafsson, and J. Edsjo, Phys. Rev. D **79**, 035013 (2009).
[47] M. Merchand and M. Sher, J. High Energy Phys. 03 (2020) 108.
[48] G. Belanger, A. Mjallal, and A. Pukhov, Phys. Rev. D **105**, 035018 (2022).